Engineering Structures 357 (2026) 122566

Contents lists available at ScienceDirect

Engineering Structures

journal homepage: www.elsevier.com/locate/engstruct

Interface test-based load transfer curves to predict the response of offshore piles subjected to drained pull-out

Giada Orlando *, Laura Govoni

University of Bologna, Viale del Risorgimento 2, Bologna 40136, Italy

ARTICLE INFO

Keywords:
Offshore piles
Load-transfer curves
CPT
Interface tests
Offshore wind

ABSTRACT

This study develops a shaft load-transfer curve formulation to predict the response of offshore piles to pull-out. The functional form is the second-order conical equation recently proposed within the PISA framework for laterally loaded piles. A procedure to identify the constants of the approach is proposed which employs the unified CPT method to determine the ultimate conditions, and results of interface tests to describe the pile monotonic response prior to failure. The formulation is devised and validated using the data of an experimental campaign on model piles, field tests and results of two-dimensional finite element analyses. The load-transfer curves are intended for piles supporting wind turbines on jackets in intermediate and deep waters, but their application can also be extended to anchor piles.

1. Introduction

Jacket structures are being increasingly used to extend offshore wind installations from shallow to intermediate water depths, either in the North Sea [1] or off the Atlantic coast [2]. A recent study has also illustrated the potential of the Adriatic Sea for offshore wind developments on jackets [3]. Jacket structures are supported mainly by steel open-ended piles. In this configuration, the foundations are predominantly subjected to axial tensile and compressive loads through a push-pull mechanism. As a result, there is renewed interest in both the research community and industry in developing robust design procedures for axially loaded piles.

Over the last two decades, various methods based on Cone Penetration Test (CPT) data were proposed to predict the ultimate axial capacity of offshore piles in sand. These procedures, comprehensively described in [4], have been recently collected under a unique approach, named Unified CPT method [5]. The method contains empirical elements but also builds upon strong theoretical bases, explicitly accounting for essential behavioural features of open-ended driven piles, such as the effects of friction fatigue [6] and degree of soil plugging [7], which occurs during the pile installation. Shown to provide excellent correlation with a large set of pile load tests performed at various locations worldwide and referred to as the Unified database [8], the Unified CPT method was incorporated in the latest ISO 19901–4 [9] to be used for ultimate limit state design of offshore piles in sand.

The pile performance under in-service conditions is routinely predicted with the load-transfer curves method, which implements the Winkler model of soil reaction and employs suitable functions to describe the stress-displacement response along the pile. The method dates back to the Sixties [10], but novel load-transfer functions continue to be developed [11–14]. For offshore piles, ISO 19901–4 [9] still recommends the use of the API curves [15] for design purposes. The main shortcomings of the API formulation were shown to relate to the prediction of the shaft response, arising from the use of a constant value for the pile displacement at failure to diameter ratio, with major limitations observed for piles tested in tension, notably in dense sand [16,17]. Other procedures, based on continuous models or numerical methods, either deterministic [18–21] or probabilistic [22,23] metamodels have also been recently considered.

For small jackets supporting lightweight wind generators, tensile loads can be particularly onerous, driving the design choices, therefore this paper introduces shaft load-transfer curves to predict the monotonic drained behaviour of offshores pile when subjected to pull-out.

The selected mathematical form is the one recently presented within the Pile Soil Analysis (PISA) framework [24,25] for laterally loaded monopiles. A procedure to identify the equation constants is proposed, using results of routine experiments, such as constant normal load (CNL) interface tests and CPT data.

The approach is developed and validated upon available results of an experimental campaign conducted at a semi-technical scale (1:5–1:10)

* Corresponding author.
E-mail addresses: giada.orlando4@unibo.it (G. Orlando), l.govoni@unibo.it (L. Govoni).

https://doi.org/10.1016/j.engstruct.2026.122566
Received 17 September 2025; Received in revised form 5 February 2026; Accepted 10 March 2026
Available online 14 March 2026

on two model piles of different embedment ratios. The problem is first addressed via a two-dimensional finite element (2D-FE) approach that implements the constitutive model of Sanisand [26] to reproduce the experiments and extrapolate the load-transfer curves. The comparison between the numerical load-transfer curves and the results of the experimentally available interface tests provides the basis for the development of interface-test based load-transfer curves, which are implemented in a one-dimensional finite element model. The outcomes of the analyses are eventually validated by comparison with the model pile test data and field test data, showing consistently good agreement.

The proposed approach delivers a t–z formulation that can be implemented in any structural analysis software but that it is grounded in a robust geotechnical theoretical framework.

2. Details of the experiments

The tests were carried by the research institute Fraunhofer IWES at the Leibniz University of Hannover and were first published in [27].

Essential details of the experimental campaign are summarised in the following.

The laboratory hosts an indoor pit of length 14 m, width 9 m and depth 10 m devised to investigate the response of offshore foundations at a semi-technical scale (1:10–1:5). A schematic drawing of the experimental set-up is given in Fig. 1

2.1. Sample preparation

The soil used in the experiments was a medium fine silica sand, named Rohsand 3152, whose physical properties are given in Table 1.

The sample was prepared in layers of average thickness 25 cm up to a final height of 9.65 m then saturated at a constant rate of 30 cm/day up to 0.5 m below the surface. Each layer was compacted using a small hand-operated vibratory plate compactor (0.16 m^2 area and peak load of 16 kN). Cone penetration tests were carried out with a cone of diameter, d_{cone}, of 25.2 mm and area of 500 mm^2. The profiles of cone resistance, q_c, are displayed in Fig. 2a, reflecting the preparation in layers characterised by almost constant amplitude oscillations about average. Peaks correspond to the top of each layer and the tails to the bottom.

Three undisturbed core specimens were retrieved from each layer after compaction, systematically varying the sampling location to cover the entire pit area. The relative densities calculated on these specimens are shown in Fig. 2b. The mean value resulted equal to 0.74 as it is also shown in Fig. 2b, with a coefficient of variation of 2.9%, assessing a rather homogeneous sample.

Table 1
Properties of Rohsand 3152.

D_{10}	D_{50}	D_{60}	C_u	C_c	USCS	e_{min}	e_{max}	G_s
[mm]	[mm]	[mm]	[-]	[-]	[-]	[-]	[-]	[-]
0.22	0.36	0.40	1.82	0.96	SP	0.44	0.83	2.70

2.2. Model piles tests

Two model piles were considered in this present study, hereinafter referred to as P3 and P4 (Fig. 1, Table 2). They were open-ended and made of S355 steel. The average centre-line roughness, R_a, was measured equal to 5 μm, with a normalised roughness $R_{t,max}/D_{50}$ of about 0.06. The installation was completed using a double-acting pile hammer, with measurements of the incremental filling ratio carried out throughout. After the installation and following a 23-day set-up, the piles were subjected to monotonic loading up to a mobilised pile displacement of 0.1D. For both piles, installation was fully cored and pull-out fully plugged. During the tests, the axial load, Q, and head displacement, w_{pile}, were recorded. Measured ultimate capacities were 195 kN for pile P3 and 258 kN for pile P4.

2.3. Operative cone resistance

The operative cone resistance profile, $q_{c,stn}$, was evaluated using the following empirical correlation, which was selected to accommodate cone size effects [28]

$$q_{c,dcone} = q_{c,1} q_{c,2} \tag{1}$$

where:

$$q_{c,1} = C_1 p' \left(\frac{p'}{p_a}\right)^{-C_2} \exp(C_3 D_r) \tag{2}$$

and

$$q_{c,2} = 1 - \exp\left[-\frac{z}{d_{cone}} \frac{C_4}{D_r^2} \left(\frac{p'}{p_a}\right)^{-C_5} \right] \tag{3}$$

where

$$p' = \sigma'_{v0}(1 + 2K_{oc})/3 \tag{4}$$

is the mean effective stress, K_{OC} is the compaction-induced earth pressure coefficient, assumed equal to 1.3, as calculated based on the

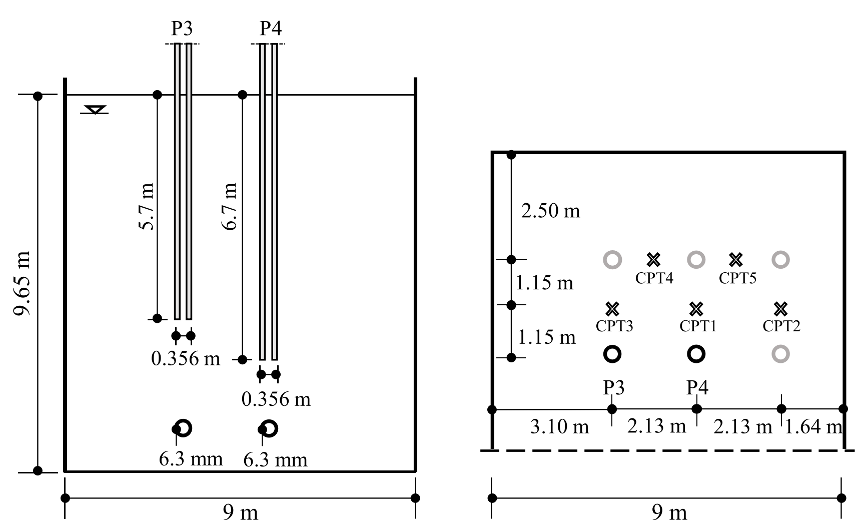

Fig. 1. Layout of the experiments.

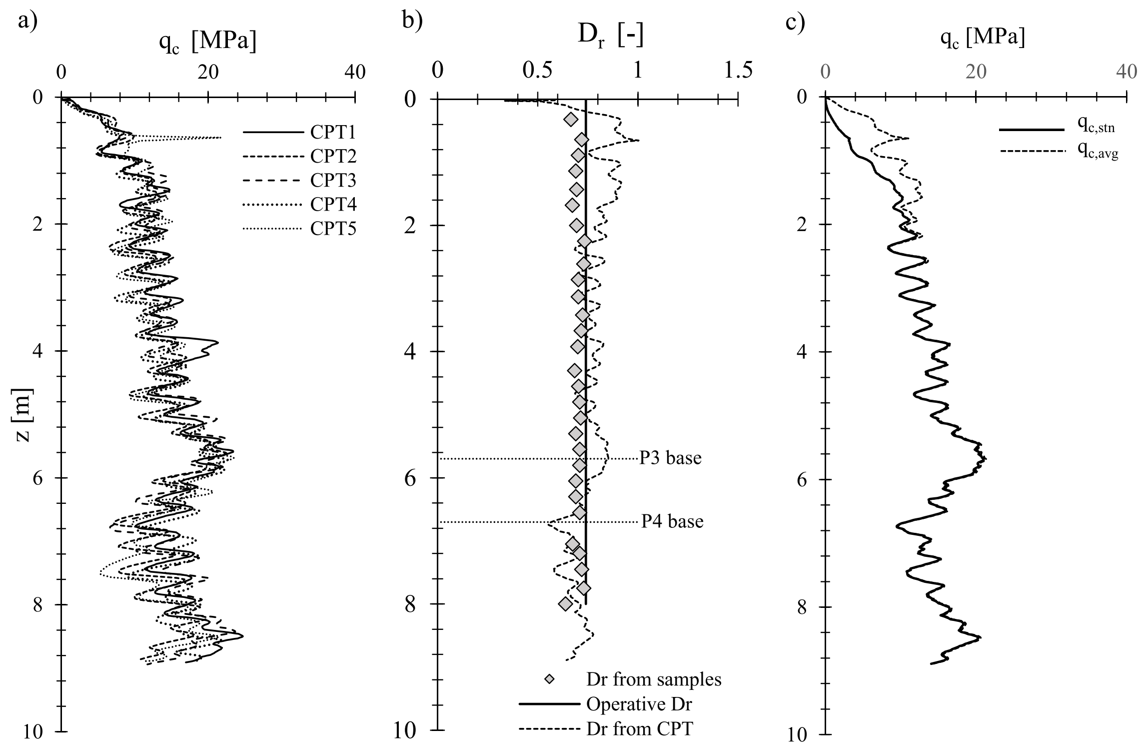

Fig. 2. Sample characterisation: profiles of a) cone tip resistance b) relative density and c) actual, ($q_{c,avg}$) and adjusted for cone size ($q_{c,stn}$) mean cone tip resistance.

Table 2
Details of the model piles.

Pile	D [m]	L [m]	s [m]	L/D [-]	D/s [-]
P3	0.356	5.70	0.0063	16.00	56.50
P2	0.356	6.70	0.0063	18.80	56.50

simplified procedure of Duncan and Seed [29] and detailed in [30], p_a is the atmospheric pressure, d_{cone} is the cone diameter, D_r is the relative density, z is the cone penetration depth and C_1, C_2, C_3, C_4, C_5 are empirical constants.

Constants $C_1 = 22$, $C_2 = 0.45$, $C_3 = 2.93$, $C_4 = 0.07$ and $C_5 = 0.5$ were those which provided the best fit to the D_r measured on specimens (Fig. 2b). The values C_4 and C_5 were close to those suggested by [28], only slightly adjusted to account for the different soil conditions [31]. To assess if the choice of the Senders [28] correlation was appropriate, the mean soil relative density near the model piles (indicated as operative D_r in Fig. 2b) was also evaluated with Eq. 1 and resulted equal to 0.74, eventually matching the laboratory-measured average.

Eq. 1 was applied again to the estimated D_r profile to convert the cone resistance measured in the laboratory with the small cone ($d_{cone} =$ 25.2 mm) to the cone resistance that would be measured employing the standard measure, $d_{CPT} = 35.7$ mm, and indicated hereinafter as $q_{c,stn}$. In Fig. 2c, the $q_{c,stn}$ profile is compared to that obtained averaging all the CPTs and indicated as $q_{c,avg}$. Main differences are found in the first one and a half meters, where the shallow failure mechanism governs the penetration [32]. The predicted standard cone profile $q_{c,stn}$ is employed when empirical correlations are applied to the evaluation of ultimate condition in the proposed 1D-model, to avoid the cone size affecting the results.

3. 2D-FE models

The 2D-FE models of the load tests were developed using the commercial FE package Abaqus 2020 [33].

3.1. Mesh geometry and boundary conditions

The model was devised in axial-symmetric conditions, imposing zero displacement boundaries at a distance of 15D from the pile shaft and 10D down the pile tip. Boundaries were set to ensure no influence on the model response at failure and prior to failure, setting a distance greater than the magic radius [34]. The mesh was generated using 4-node bilinear axisymmetric quadrilateral elements (CAX4) which are recommended for analyses involving relatively large displacements. This element type also reduces CPU time compared with higher-order elements, while maintaining adequate accuracy [33]. Mesh geometry is shown in Fig. 3.

A structured mesh was used for the pile, with elements of width D/40 and aspect ratio of 10. For the soil, a structured mesh was also used throughout the domain but it was replaced by a free mesh of quadrangular elements up to 3D from the pile shaft and 3D from the base to smooth the transition from very thin to thicker elements. A check on possible distorted elements was completed before the analyses, to avoid convergence problems. The mesh was created following the operative indications of [35], as they provided a good balance between accuracy and computational costs for axially loaded piles (in this present study, about 90 min using a standard processor – e.g. i9–13900H, 2.60 GHz). A thin column of rectangular elements was inserted next to the pile shaft to model the pile-soil interface as further detailed in Section 3.3.

3.2. Soil and piles modelling

The piles were wished-in-place and modelled with deformable elements to which a linear-elastic behaviour was assigned. As a fully plugged failure was experimentally observed after a cored penetration, the pile cross section was assumed uniform and the density and elastic properties were calculated as equivalent to the actual open-ended one ($E_{pile} = 9.14$ GPa and $\nu = 0.3$). To the soil, the Sanisand constitutive model in the version proposed by Dafalias and Manzari [26] was

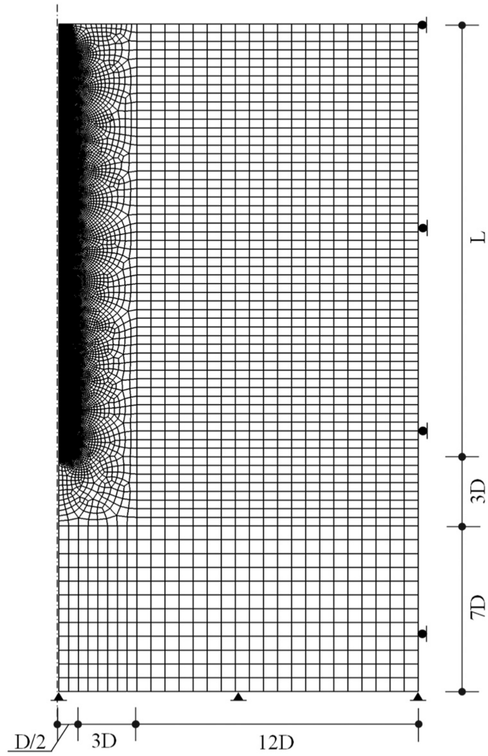

Fig. 3. Two-dimensional finite element mesh.

assigned by implementing an external subroutine. The model constants were calibrated on isotropically consolidated drained triaxial tests conducted on Rohsand 3152 samples for different levels of confining stresses. Further details on the calibration are provided in [36] and constants are listed in Table 3. A relative density was prescribed to the domain equal to the experimental average (e = 0.541).

3.3. Contact formulation and interface modelling

The contact between the pile base and the soil was modelled using the software's hard contact algorithm, which prevents the transfer of tensile stresses across the interface [33]. A thin column of rectangular elements, herein referred to as interface elements, of width μD_{50}, was inserted next to the pile shaft to model the pile-soil interface, with D_{50} being the sand mean particle diameter and μ the dimensionless interface thickness. Interface element thickness was selected based on previous empirical observations on shear band formation in experimental setups. For a medium-fine silica sand (D_{50}=0.36 mm) in contact with steel surfaces of roughness $R_a = 5$ μm and $R_{t,max}/D_{50}$ of about 0.06, a value of $\mu = 5$ appeared to be a reasonable modelling choice [37]. Instead, the height of interface elements was set equal to 10μ, as this allowed for an accurate description of interface kinematics (further detailed in Section 4.2) while also preventing convergence issues. This choice also aligns with the aspect ratio range recommended for finite-thickness interface elements by [38]. A perfect contact was assigned between the pile and the adjacent interface elements, by tying together their common nodes with respect to all degrees of freedom. The advantage of using two-dimensional interface elements over the zero-thickness ones is that no additional algorithms are needed and standard FE rectangular elements can be employed as long as their behaviour is described by a suitable constitutive law [19].

The interface elements were prescribed to behave according to the Sanisand constitutive model but with constants adjusted to best fit the results of the available interface tests. The experiments used were Constant Normal Load (CNL) interface shear tests carried on samples of Rohsand 3152 and employing steel plates of $R_a = 5$ μm and $D_r = 0.74$. The tests were performed by the same laboratory facility that tested the piles and data already published in [36].

To identify the constants of the interface constitutive model, a four-node bi-linear plane strain quadrilateral element of thickness $5D_{50}$ was implemented in Abaqus to simulate the experimental CNL test. The void ratio was set to prescribe a 0.74 relative density to the element at the beginning of the shear phase (e = 0.541). Movements were fully restrained at the element base while the upper edge was free to move. The confining stress was assigned as a uniform normal pressure, σ'_v, matching the experimental values (30 kPa, 90 kPa). Shear was applied in a displacement-controlled way up to 8 mm. In Figs. 4a and 4b, the evolution of the experimental shear stresses, τ, and vertical displacements, y, with the applied horizontal displacements, x, are compared with the outcome of the FE analysis. The comparison shows a rather satisfactory agreement on mobilised shear stresses, albeit with a slightly reduced peak and a smaller initial compression, aspects that, as shown in Section 4, did not particularly influence pile response. The model constants for the interface elements are also listed in Table 3.

4. 2D-FE analyses

The 2D-FE analyses started with the application of the geostatic step, during which the stress field was initialised by assigning uniformly a value of earth pressure coefficient K= 1.2 that accounted for the effects of sample compaction and pile installation following the indication of [39] for medium rough pile installed in medium to dense samples ($R_{t,max}/D_{50}$~0.06). The procedure of incorporating the installation effect in wished-in-place piles was already successfully applied in previous FE studies (e.g. [38] and [40]).

After this step, an upward vertical displacement of 0.1D was applied to the pile head. Loading analyses were monotonic conducted with quasi-static implicit dynamic simulations.

4.1. Pile response

Numerical simulations ended when failure conditions were reached in all interface elements and the pile base completely detached from the surrounding soil as shown in Figs. 5a and 5c. The results of the analyses are shown in terms of load-displacement curves in Fig. 5a along with the corresponding experimental data for pile P3; those referred to pile P4 are displayed in Fig. 5c. The numerical results closely approximate the experimental data for both piles. After an initial non-linear branch, along which most of the ultimate capacity was mobilised, the axial load continued to increase slightly and almost linearly as the piles were pulled out until flattening into a plateau. The focus on the initial curve branch, provided in Figs. 5b and 5d, confirms the ability of the model to reproduce the experimental response at working loads, defined as those within the 50% of the ultimate capacity. The curves obtained with the

Table 3
Sanisand [26] parameters sets.

	e_{c0}	λ	ξ	M_c	M_e	m	$\overline{G_0}$	ν	h_0	c_h	n^b	A_0	n^d	c_z	z_{max}
	[-]	[-]	[-]	[-]	[-]	[-]	[-]	[-]	[-]	[-]	[-]	[-]	[-]	[-]	[-]
Soil	0.62	0.015	0.40	1.31	0.911	0.02	200	0.05	5	0.968	1.4	0.9	2.5	0	0
Interface Elements	0.62	0.015	0.40	1.07	0.789	0.02	5	0.05	5	0.968	0.8	0.22	3.5	0	0

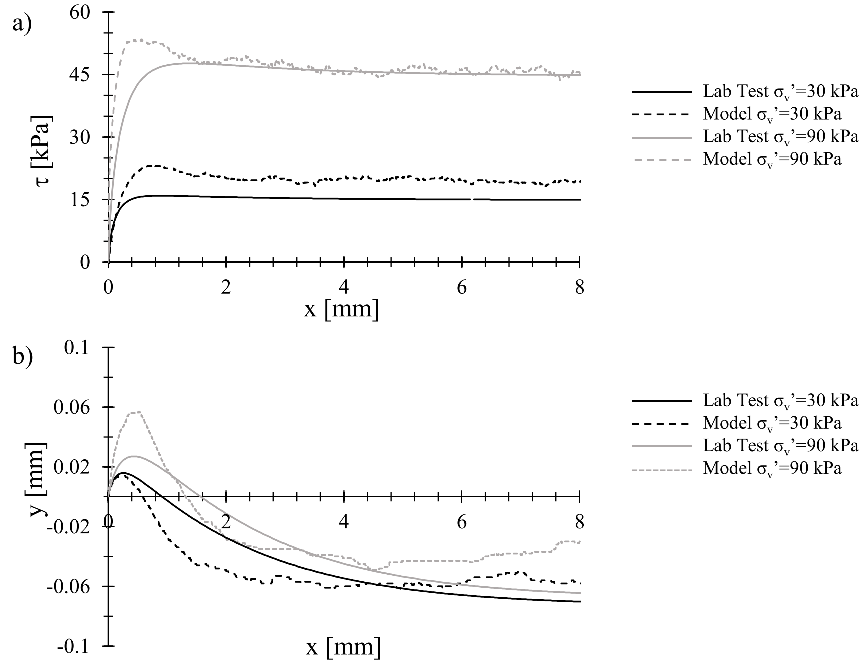

Fig. 4. Constant normal load interfaces test results conducted at different vertical confinement stresses, σ'_v.

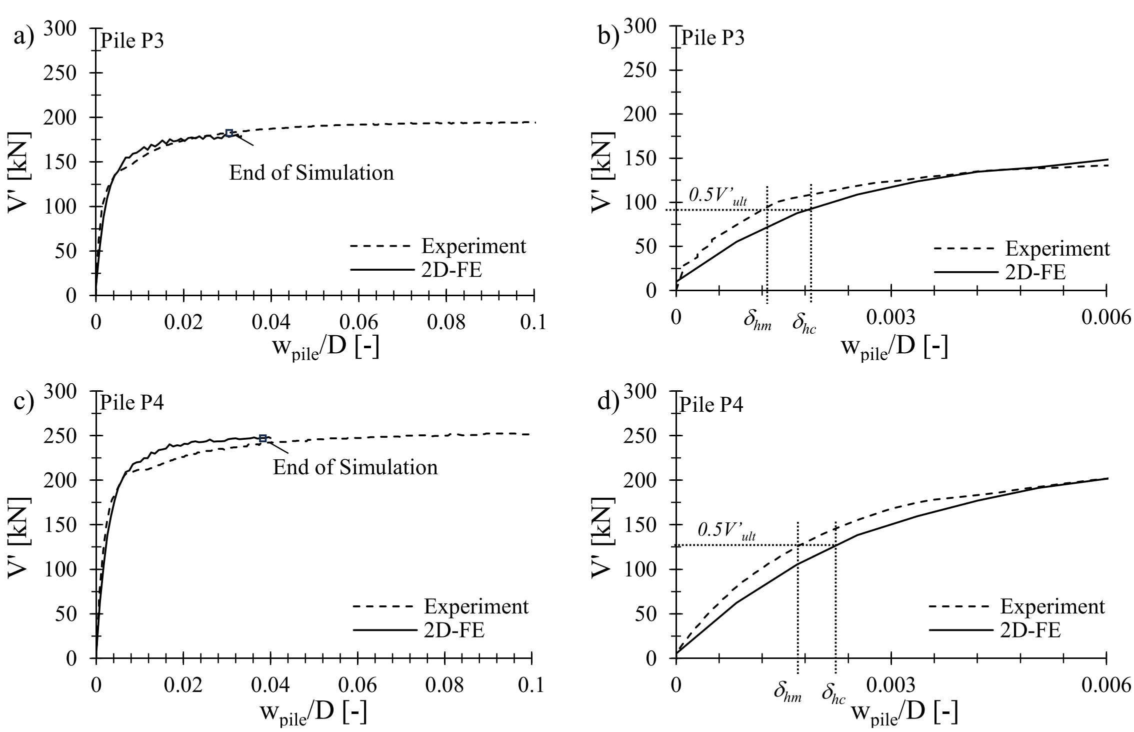

Fig. 5. Results of the 2D-FE analyses compared with experimental data: a) load-displacement response for pile P3 and b) focus on working load and relative measured (δ_{hm}) and computed (δ_{hc}) pile head displacements for pile P3, c) load-displacement response for pile P4 and d) focus on working load and relative measured (δ_{hm}) and computed (δ_{hc}) pile head displacements for pile P4.

2D-FE model closely follow the experimental ones and provide rather accurate prediction of working load displacements. The introduced error, defined as the difference between the measured pile head displacement, δh_m, and calculated head displacement, δh_c, both mobilised at the 50% of the ultimate capacity, was lower than 0.5%D [17].

4.2. Interface behaviour

Fig. 6 illustrates the interface response at failure. In particular, with reference to a selection of eleven (thirteen) interface elements along pile P3 (P4), Fig. 6a (6b) displays the shear stress, τ, and the corresponding radial stress, σ'_r, on the shaft, throughout the last steps of the analysis. As it is observed, all elements have reached the critical state line of

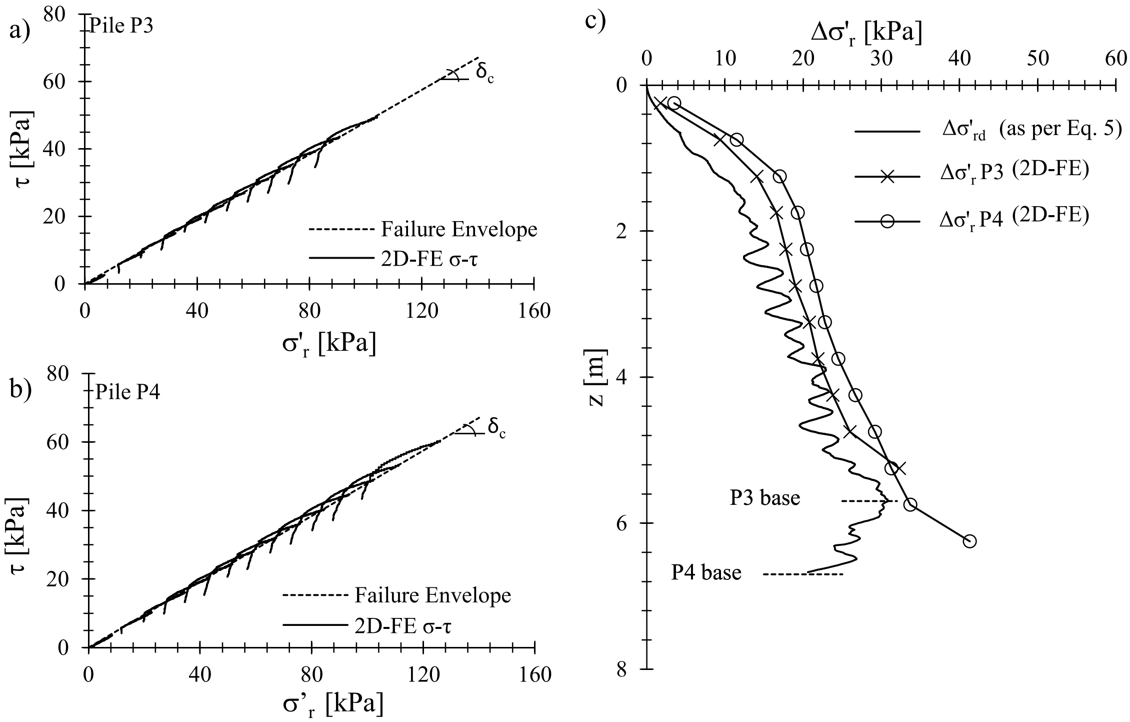

Fig. 6. Results of the FE analyses a) stress paths along the shaft for pile P3 and b) for pile P4; c) evolution with depth of the increment in radial stress at failure for pile P3 and P4.

inclination $\delta_c = 27^\circ$ along the vertical plane, following the mobilisation of a slight peak shaft friction.

Fig. 6c also shows results taken at the end of the analysis, given in terms of increment of radial stress, $\Delta\sigma'_r$, and pile depth along with the prediction of the unified CPT method

$$\Delta\sigma'_{rd} = \left(\frac{q_c}{10}\right)\left(\frac{q_c}{\sigma'_{v0}}\right)^{-0.33}\left(\frac{d_{CPT}}{D}\right) \tag{5}$$

where d_{CPT} is the standard cone diameter, and $q_c = q_{c,stn}$ as introduced in Section 2.1.

The trend of the numerical and empirical predictions is close, exhibiting a non-linear increase with depth. This rise in radial stress is due to inhibited dilation along the pile shaft by the surrounding soil, also leading to the development of the peak friction angles observed in Figs. 6a and 6b. This might explain the slight discrepancy observed in the comparison in Fig. 6c. In fact, a larger dilation, and thus a larger increase in the radial stress, is expected for pile P3 and pile P4 with respect to that predicted by Eq. 5, which was developed on piles of comparatively higher dimensions [8].

The evolution of radial stress along the pile shaft is traditionally interpreted through the cavity expansion (CE) theory as follows

$$\Delta\sigma'_{r,CE} = \frac{4G}{D}y \tag{6}$$

where y is the sand dilation. According to [41], the operational shear modulus G can be calculated combining the following equations

$$G = \frac{G_0}{1 + \left(\frac{2y/D}{0.0001}\right)^{\alpha}} \tag{7}$$

and

$$y = \frac{y_0}{1 + \left(\frac{k_n}{k_{n,ref}}\right)^{\alpha}} \tag{8}$$

where G_0 is the small strain stiffness, y_0 is the maximum value of dilation measured in CNL interface test, $k_n = 4\ G/D$ is the normal stiffness of the far field soil [42], $k_{n,ref}$ and α are the constants of the equations equal to 500 kPa/mm and between 0.4 and 0.7, respectively.

With reference to pile P3, Fig. 7 depicts shear and normal stiffness acting along the pile during the FE analysis.

In particular, Fig. 7a shows the operational shear stiffness, G, at the end of the simulation along with the prediction of Eq. 7. For the calculation, the value of y_0 was taken as the maximum dilation measured in the FE CNL interface tests which were completed to this scope, assigning confining stress values equal to those expected acting on the pile shaft prior to loading. The small-strain stiffness, G_0, was instead estimated using the Sanisand constitutive equation [43,44]. For the piles in exam, cavity strains were observed to be sufficiently large, so that G values at failure became significantly lower than G_0, whose profile with depth is also inserted in Fig. 7a. In fact, the value of α which led to the best fit of Eq. 7 to the numerical G is 0.4, on the lowest boundary of Eqs. 7 and 8, in agreement with the observed larger increase in radial stress, depicted in Fig. 6c.

Fig. 7b shows the evolution of normal stiffness throughout the simulations at various depths, with reference to the dilation phase only. The steeper part of the curves corresponds to the transition from the initial contraction phase. The stiffness increases with depth and tends to stabilise to a constant value at relative displacements which also increase with depth, assessing that the stress path along the pile shaft is close to normal stiffness, although not precisely so [45].

5. Development of load-transfer curves

Load-transfer curves, in terms of the mobilised shear stress, τ, and vertical displacement, w (calculated relatively to the pile movement at various pile depths), were extracted at each interface element and then averaged upon layers of length equal to 0.51 m.

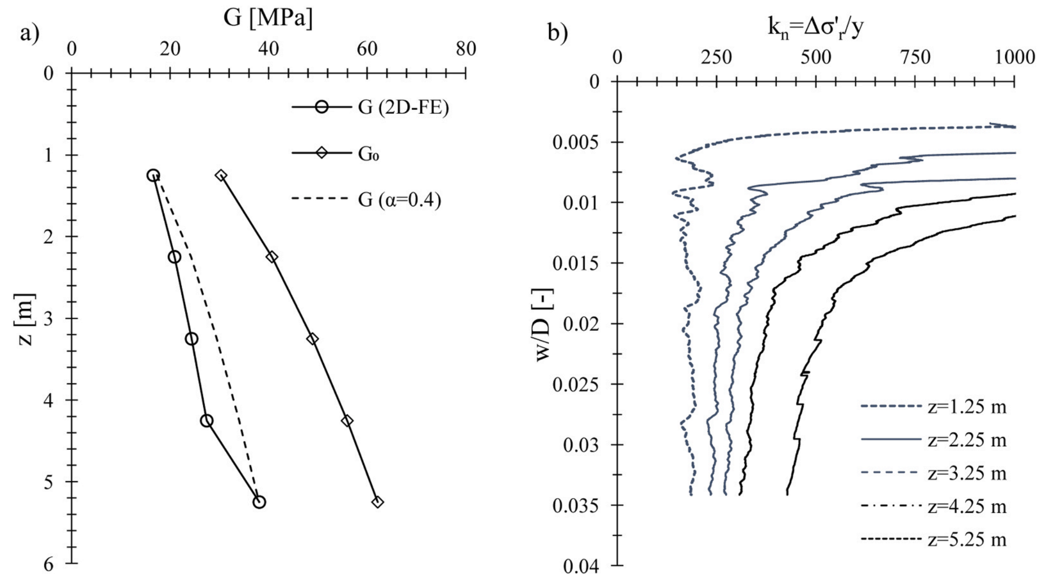

Fig. 7. FE shear and normal stiffnesses acting along pile P3, a) evolution with depth of the operation shear modulus at failure and b) evolution of normal stiffness throughout the simulations at various depths.

5.1. Load transfer curves and CNL interface tests results

A selection of the extracted load-transfer curves given at various pile depths is shown in Fig. 8a, for pile P3 and Fig. 8b for pile P4, with reference to the corresponding initial radial stress, σ'_{ri}. The shape of the curves is similar, independent of the pile dimensions and depth. A hardening type of response is observed with the shear stress monotonically increasing up to the end of the analysis.

In Fig. 8c, the results of a set of FE CNL interface tests are displayed in terms of mobilised shear stress, τ, and horizontal displacement, x. These tests were performed using the single-element model described in Section 3.3 and assigning values of confining stress, σ'_v, in the range of those acting on the pile shaft prior to loading, σ'_{ri}, (i.e. from ten to 80 kPa). Different from the response observed along the pile shaft, the CNL curves exhibit a small peak before reaching the steady state. Dividing the shear stress by the mobilised normal stress, variable along the pile shaft (σ'_r) and constant (σ'_v) in the interface tests, load-transfer curves and CNL results align rather closely, as it shown in Fig. 9, where data are displayed against the respective vertical, w, and horizontal displacement, x.

The agreement is observed along the entire curves, from the initial linear branch to the attainment of a steady state. When normalised, a small peak is observed also in the 2D-FE curves mostly in those related to shallowest layers. This outcome provides the base for the development of load-transfer curves as described in Section 5.2

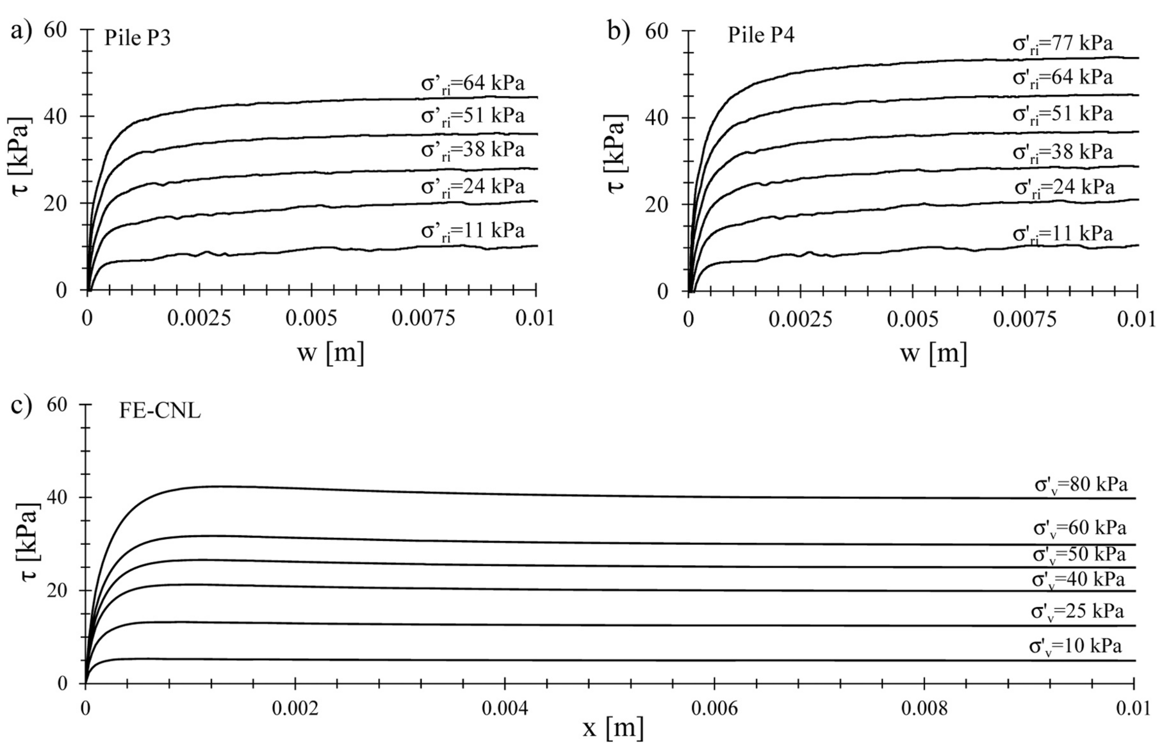

Fig. 8. FE load-transfer curves, a) at various depths along the shaft of pile P3, b) at various depths along the shaft of pile P4 and c) results of FE interfaces tests.

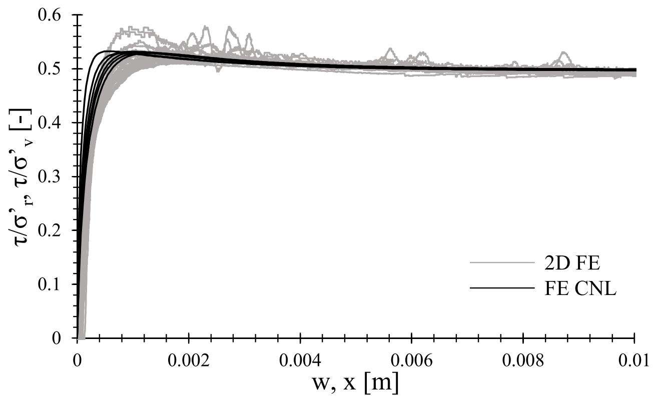

Fig. 9. Friction mobilised with displacement in the 2D-FE analyses and FE CNL interface tests.

5.2. Functional form

The second-order conical function, proposed within the PISA framework [24], proved particularly suitable for describing the curves shown in Figs. 8a and 8b. This is because post-peak strain softening was not observed, as expected for load transfer in sand [17].

The PISA equation was, therefore, rewritten as follows

$$-n\left(\frac{\bar{t}}{\overline{t_u}}-\frac{\bar{w}}{\overline{w_u}}\right)^2+(1-n)\left(\frac{\bar{t}}{\overline{t_u}}-\frac{\bar{w}K}{\overline{t_u}}\right)\left(\frac{\bar{t}}{\overline{t_u}}-1\right)=0, \quad \bar{w}<\overline{w_u} \tag{9}$$

where $\bar{t}$ and $\bar{w}$ are the normalised shear stress, τ, and displacement, w, variables and $\overline{t_u}$, $\overline{w_u}$, K and n are the model parameters.

In Eq. 9, $\bar{t}$ is divided by the initial radial confining stress, σ'_{rc}, computed as per [5]:

$$\sigma'_{rc}=\frac{q_c}{44}\left[1-\mathrm{PLR}\left(\frac{D-2s}{D}\right)^2\right]^{0.3}\left[\max\left(1,\frac{L-z}{D}\right)\right]^{-0.4} \tag{10}$$

where s is the pile wall thickness and L is the pile length.

Variable $\bar{w}$ is by divided by $\mu D_{50}^2/R_a$. For industrial steel tubular piles installed in coarse-grained soil μ values are in the rage 3–5 [39].

The parameter $\overline{t_u}$ is the normalised ultimate shear stress, τ_u/σ'_{rc}, estimated also as per Lehane et al. [5]

$$\overline{t_u}=\frac{\tau_u}{\sigma'_{rc}}=0.75\left(1+\frac{\Delta\sigma'_{rd}}{\sigma'_{rc}}\right)\tan 29^{\circ} \tag{11}$$

where,$\Delta\sigma'_{rd}$ is calculated according to Eq. 5.

The ultimate normalised displacement, indicated as $\overline{w_u}$, is the value at which the ultimate shear stress is attained.

Parameter K is the initial slope of the load-transfer curves and can be expressed as function of $\Delta\sigma'_{rd}$ as follows

$$K=k\left(1+\frac{\Delta\sigma'_{rd}}{\sigma'_{rc}}\right) \tag{12}$$

where k is a dimensionless constant. The curvature of the function is defined by n, with $0 \le n \le 1$.

Fig. 10 schematically depicts the procedure to identify the model constants from CNL tests.

The results of the experiments, carried out at values of normal stress relevant to the pile depth ($\sigma'_v = \sigma'_{rc}$), are plotted in terms of $\bar{t}$ against the horizontal displacement, x, normalised by $\mu D_{50}^2/R_a$, $\bar{x}$. Possible gaps in the experimental results can be filled using suitably calibrated numerical models as illustrated in Section 3.3 or shown in Fig. 8c.

On the graph, $\overline{w_u}$ is taken as the ultimate normalised horizontal displacement, $\overline{x_u}$, which corresponds to the attainment of the curves' steady state, based on the correspondence between w and x shown in

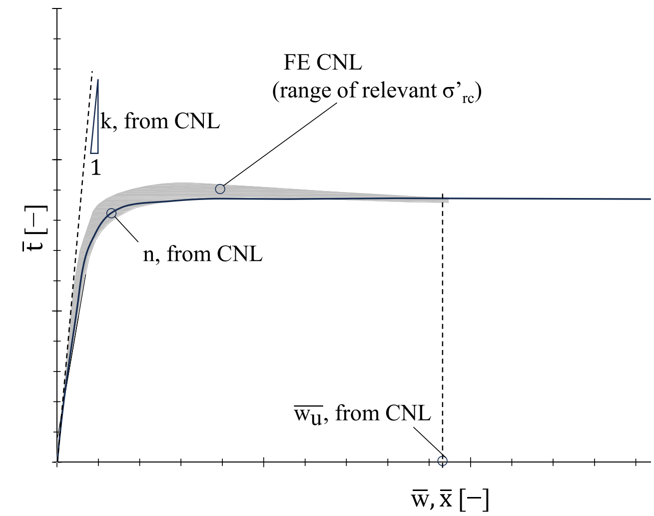

Fig. 10. Schematic drawing of the procedure to identify the model constants from CNL tests.

Fig. 9. The dimensionless constant, k, is obtained by interpolation of the first linear branch of the curves and the curvature n is evaluated following a fitting of all the interface tests data using the Gauss-Newton non-linear least square approach. As anticipated, Eq. 9 does not allow for the modelling of post-peak strain softening, therefore peak values, if present, are cut out by the interpolation. The diagram present in Fig. 11 schematically illustrates the step-by-step workflow to implement when using the proposed t-z model.

5.3. Retrospective simulations of the experimental results using a one-dimensional FE model

The procedure described in Section 5 was applied to predict, retrospectively, the response of piles P3 and P4 using a one-dimensional 1D-

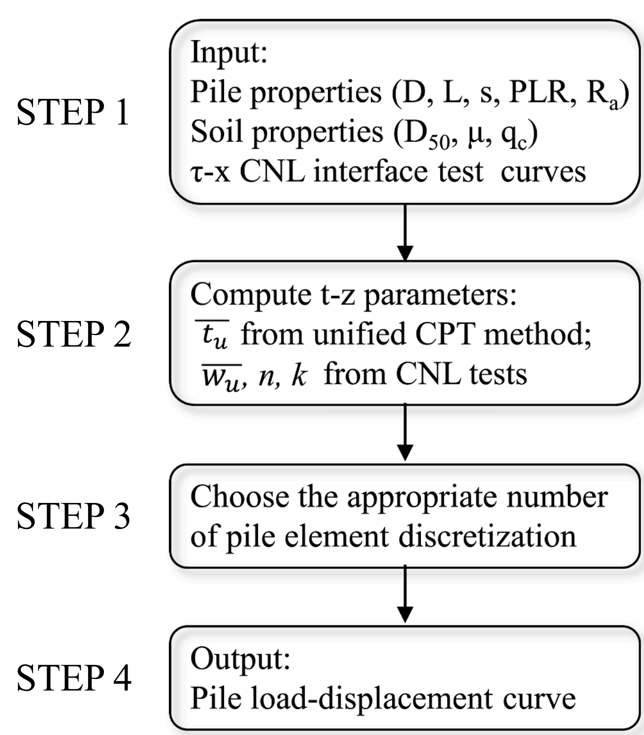

Fig. 11. Workflow diagram to implement the proposed t-z model.

FE models which were also implemented in Abaqus.

The piles were modelled using truss elements 0.25 m long. The number of elements was identified following a sensitivity analysis that showed no variations in the results to further mesh refinements. To each element, the equivalent elastic constants already used in the 2D-FE model were prescribed to account for the effects of the composite steel-soil pile section on the pile axial stiffness.

For the soil reaction, non-linear elastic springs were attached to each element midpoint, to which Eq. 9 was assigned with parameters $\overline{w_u}$= 0.05, k = 640, n = 0.95. The ultimate normalised shear stress $\overline{t_u}$ was computed using Eq. 11 at each element midpoint. A vertical displacement of 0.1D was applied to the pile head.

Fig. 12 shows the load against relative displacement curves obtained with the 1D-FE model along with their corresponding test results. Specifically, outcomes referred to Piles P3 are reported in Figs. 12a and 12c, while those for Piles P4 are presented in Figs. 12b and 12d.

Throughout the entire test, the numerical curves track closely the experimental ones. An excellent agreement is observed at failure, assessing the ability of the CPT method to reproduce the pile ultimate capacity in tension.

In fact, the values obtained with the proposed approach were 202 kN for pile P3 and 250 kN for pile P4, introducing an error of the 8% for pile P3 and 0.8% for pile P4.

The procedure used for the development of the load-transfer curves also revealed effective to model the pile behaviour prior to failure. This can be appreciated in the focus of Figs. 12b and 12d for piles P3 and P4, respectively. The difference between the measured pile head displacement, δh_m, and calculated head displacement, δh_c, both mobilised at 50% of the ultimate capacity, as suggest by [17], resulted in an associated error, $(\delta h_c - \delta h_m)/D$ below 0.5%D for both piles.

In Fig. 12, the results are also compared to the prediction obtained employing the API [15] load-transfer curves. The API [15] equation uses non-modifiable stiffness and curvature parameters and does not allow for adjustment to account for sand and pile specificities. For the piles in exam, the use of the API [15] load-transfer curves resulted in an underestimation of the response prior to failure (Figs. 12a and 12b) and in a prediction of a more compliant behaviour at small pile head displacements as it is observed in Figs. 12b and 12d.

5.4. Application to a well-documented case study

Results of field tests on two open-ended pipe piles were used to assess the ability of the approach to reproduce the pile behaviour in site conditions. Experimental data are taken from well-documented field tests located on the French shore at Dunkirk. Offshore piles are traditionally tested in onshore locations, and with reduced geometries, due to the difficulties, economic disadvantages and regulation restrictions of testing underwater in an offshore location. The selected piles are, therefore, benchmark cases with slenderness ratios much higher than those tested in indoor facilities and are the Dunkirk CLAROM – CL reported in [46] and the Dunkirk GOPAL – R1 reported in [47], whose geometries are listed in Table 4.

The piles are driven in a rather homogeneous formation of dense Flandrain sand (D_{50}=0.26 mm, e_{min}=0.5, e_{max}=0.9, D_r =75%). CPT tests were carried out on site, the typical q_c profile, reported in [46], is depicted in Fig. 13a together with its interpolation by means of Eq. 1 used for calculation.

Soil-steel CNL interface tests were carried out on samples of Dunkirk sand using a steel plate of R_a= 10 μm and with a normal confinement σ'_n= 150 kPa. Result of the interface direct shear test redrawn from [46] and concerning a dense sample used for t-z parameter calibration is reported in Fig. 13b. The ultimate normalised displacement resulted in $\overline{w_u}$= 0.02, the point after which no further data oscillations were observed. The initial stiffness factor was k = 45 and the curvature

Table 4
Details of the selected piles tested at the Dunkirk site.

Pile	*D* [m]	*L* [m]	*t* [m]	*L/D* [-]	*D/t* [-]	PLR [-]
CLAROM – CL	0.324	11.30	0.0127	34.87	25.50	0.55
GOPAL – R1	0.457	19.30	0.0135	42.23	33.85	0.60

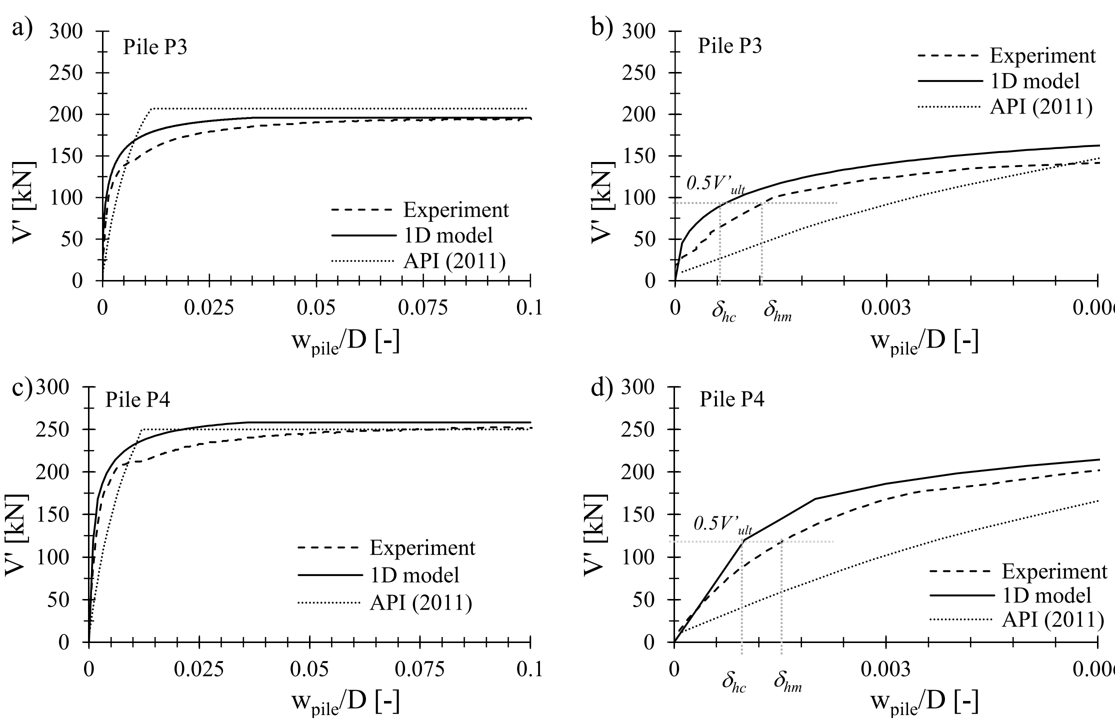

Fig. 12. 1D FE results compared with experimental data and API [15] prediction, pile response for: a) pile P3 and b) pile P3, focus on working loads displacements, c) pile P4 and d) pile P4, focus on working loads displacements.

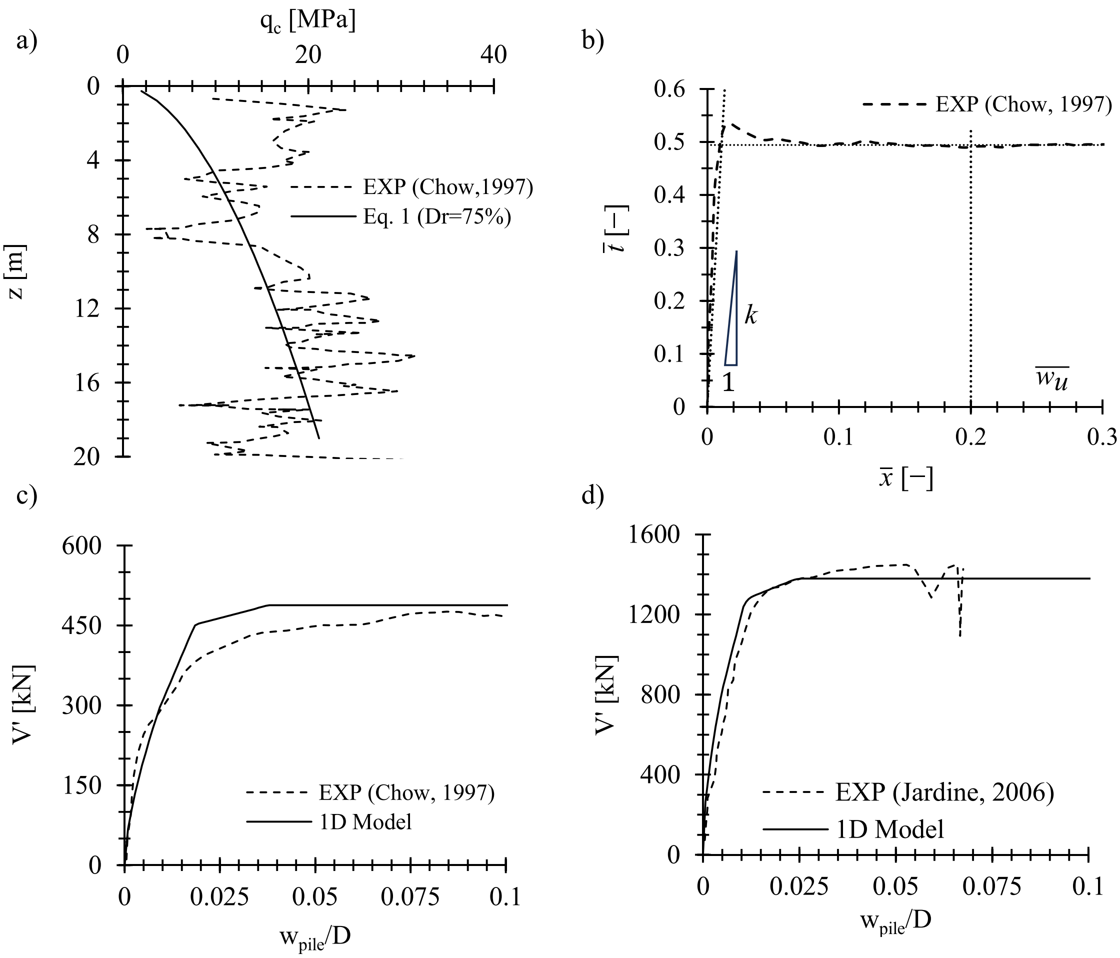

Fig. 13. Application of the framework to field tests of offshore piles: a) CPT tests, b) CNL interface tests, c) 1D model results for the Dunkirk CLAROM – CL pile and d) 1D model results for the Dunkirk GOPAL – R1 pile.

$n = 0.97$, following the procedure illustrated in Section 5.2 for parameters identification.

The ultimate normalised shear stresses were computed over layers of 0.52 m long and for PLR ratios listed in Table 4. The Dunkirk CLAROM–CL pile was, therefore, divided in 22 layers while the Dunkirk GOPAL–R1 pile was divided in 37 layers.

The same number of truss elements were used to discretise the piles in the 1D-FE model. It was again verified that the layer length was appropriate through a sensitivity analysis and further discretisation provided no increase in the result accuracy. Equivalent elastic constants ($E_{pile,CL} = 31.7$ GPa, $E_{pile,R1} = 24.18$ GPa and $\nu = 0.3$) were assigned to each element. Figs. 13c and 13d show the 1D model results together with the experimental load-displacement curves for pile CLAROM – CL and Dunkirk GOPAL – R1 respectively.

A satisfactory agreement was achieved between the 1D numerical load-displacement curves and the experimental results, particularly in terms of initial stiffness, backbone response and ultimate capacity.

The upward resistance V' predicted using the proposed approach was 488 kN for pile CLAROM–CL (experimental 467 kN) and 1380 kN for pile GOPAL–R1 (experimental 1427 kN), corresponding to errors of 4.0% and 3.2%, respectively.

The difference between the measured and calculated pile head displacement mobilised at 50% of the ultimate capacity resulted in an associated error below 0.5%D for both piles. Minor discrepancies are ascribable to the adoption of a uniform q_c profile, which neglected the denser soil layer in the first three meters and the 0.6 m thick organic lens located at a depth of 7.6 m depth (Fig. 13a). In addition, the load-transfer curve parameters were calibrated based on a single CNL interface test; a larger experimental dataset is expected to further improve the predictive accuracy.

6. Concluding remarks

The paper developed a formulation for shaft load-transfer curves for offshore piles subjected to axial tensile loading in sand, which makes use of CPT data and results of interface tests. The study is essentially procedural and was aimed at employing industry-acknowledged approaches and routinely performed site and laboratory tests. Results of 2D-FE analyses were used in combination with the data of available model pile tests to this scope.

The mathematical form that was selected is the second-degree conical function of the PISA approach, written in terms of normalised shear stress, $\bar{t}$, and of normalised displacement $\overline{w}$, and governed by four parameters ($\overline{t_u}$, $\overline{w_u}$, n, k). The normalised ultimate shear stress, $\overline{t_u}$, was computed using the unified CPT method. The normalised ultimate displacement, $\overline{w_u}$, the curvature, n, and stiffness coefficient, k, were identified on the CNL tests data, pursuing the analogy between the shear stresses mobilised in interface experiments and along the pile shaft. The load-transfer curves were implemented in a 1D-FE model which was used retrospectively to predict the outcomes of the model pile tests, yielding accurate results.

It is worth noticing that the 2D-FE analyses were used to develop the procedure but are not required for its implementation. However, FE models might be used to fill the gap of available interface experiments providing enough data to an accurate calibration of the load-transfer constants.

The procedure was verified on two simi-technical scale piles tested indoor and on two large scale field tested piles. In both cases piles were open-ended pipe-piles, intended for offshore application, driven in dense silica sand.

The proposed methodology provides t–z formulation that can be readily implemented in any structural analysis software but that it is grounded in a robust geotechnical theoretical framework.

The study was motivated by the need to extend offshore wind installations from shallow to intermediate water depths wind and therefore addresses piles for turbines on jackets. However, its application can be extended to anchor piles for deep-water developments.

CRediT authorship contribution statement

Giada Orlando: Writing – original draft, Investigation, Formal analysis, Data curation, Conceptualization. **Laura Govoni:** Writing – review & editing, Writing – original draft, Supervision, Methodology.

Declaration of Competing Interest

The authors declare that they have no known competing financial interests or personal relationships that could have appeared to influence the work reported in this paper.

Acknowledgement

Aligi Foglia and his colleagues of the Department of Support Structures of the Fraunhofer IWES are gratefully acknowledged as they have provided the data to the authors and supported in their interpretation. The authors would also like to thank the scientific staff of SoilModels (soilmodels.com) for providing the Abaqus subroutine used in this work.

Data availability

Data will be made available on request.

References

[1] Barbosa P, Geduhn M, Jardine RJ, Schroeder FC, Horn M. Offshore pile load tests in chalk. Proceeding of the 16th European Conference Soil Mechanics Geotechnical Engineering. ESSMGE 2015, Edinburgh, Scotland. 2015. p. 2885–90.

[2] DeGroot DJ, Westgate ZJ, Yetginer-Tjelta TI. Geological and geotechnical challenges of the East Coast United States for offshore energy transition. Proceedings of the 9th International Conference of Offshore Site Investigation Geotechnics. London, UK: OSIG; 2023. p. 82–111. https://doi.org/10.3723/CBKB5668.

[3] Orlando G, Govoni L, Pontani N, Panico AF, Murianni A. A database for the offshore geotechnical site characterization of Italian seas. Proceedings of the 5th International Symposium on Frontiers in Offshore Geotechnics. Nantes: ISFOG25; 2025.

[4] Lehane BM, Xu X, Schneider JA. A review of design methods for offshore driven piles in siliceous sand (GEO 05358). Perth, Australia: University of Western Australia; 2005.

[5] Lehane B, Liu Z, Bittar E, Nadim F, Lacasse S, Jardine RJ, Carotenuto P, Jeanjean P, Rattley M, Gavin K, Haavik J, Morgan N. A new "unified" CPT-based axial pile capacity design method for driven piles in sand. Proceedings of the 4th International Symposium of Frontiers in Offshore Geotechnics. Austin, Texas: ISFOG; 2020. p. 462–77.

[6] Lehane BM, Jardine RJ, Bond AJ, Frank R. Mechanisms of shaft friction in sand from instrumented pile tests. J Geotech Eng 1993;119(1):19–35. https://doi.org/10.1061/(ASCE)0733-9410(1993)119:1(19).

[7] White DJ, Lehane BM. Friction fatigue on displacement piles in sand. Géotechnique 2004;54:645–58. https://doi.org/10.1680/geot.2004.54.10.645.

[8] Lehane BM, Lim J, Carotenuto P, Nadim F, Lacasse S, Jardine RJ, Dijk BFJ. Characteristics of unified databases for driven piles. Proceedings of the 8th International Conference Offshore Site Investigation and Geotechnics. London, UK: OSIG; 2017. p. 162–91.

[9] ISO. ISO 19901-4: Petroleum and natural gas industries – specific requirements for offshore structures. Part 4. Geotechnical and foundation design considerations. Switzerland: International Standards Organisation; 2020.

[10] Fellenius BH. Discussion of axial pile load transfer curves based on instrumented load tests. J Geotech Geoenviron Eng 2018;144(4):07018005.

[11] Abchir Z, Burlon S, Frank R, Habert J, Legrand S. t–z curves for piles from pressuremeter test results. Géotechnique 2016;66:137–48. https://doi.org/10.1680/jgeot.15.P.097.

[12] Bateman AH, Crispin JJ, Vardanega PJ, Mylonakis GE. Theoretical t-z curves for axially loaded piles. J Geotech Geoenviron Eng 2022;148(7):04022052. https://doi.org/10.1061/(ASCE)GT.1943-5606.0002753.

[13] Bohn C, Santos AL dos, Frank R. Development of Axial Pile Load Transfer Curves Based on Instrumented Load Tests. J Geotech Geoenviron Eng 2017;143(1):04016081. https://doi.org/10.1061/(ASCE)GT.1943-5606.0001579.

[14] Cheng X, Vanapalli SK. Simplified approaches for predicting the nonlinear load-displacement response of single pile and pile groups in unsaturated soils. J Rock Mech Geotech Eng 2025;17:3107–24. https://doi.org/10.1016/j.jrmge.2024.10.011.

[15] API. ANSI/API RP 2GEO: Geotechnical and foundation design considerations. ISO 19901-4:2003 (modified), Petroleum and natural gas industries-specific requirements for offshore structures, Part 4 — Geotechnical and foundation design considerations. Services. Washington, DC, USA: API Publishing; 2011.

[16] Foglia A, Wefer M, Forni F. Large-scale experiments and load transfer analysis of piled foundations supporting an offshore wind turbine. Proceedings of the 8th International Conference Offshore Site Investigation and Geotechnics. London, UK: OSIG; 2017. p. 1078–83.

[17] Lehane BM, Li L, Bittar EJ. Cone penetration test-based load-transfer formulations for driven piles in sand. Géotechnique Lett 2020;10:568–74. https://doi.org/10.1680/jgele.20.00096.

[18] Garcia JR, De Albuquerque PJR, Dos Santos PRC, De Freitas Neto O. Analysis of the behavior of piled foundations in unconventional soil. Eng Struct 2024;319:118832. https://doi.org/10.1016/j.engstruct.2024.118832.

[19] Said I, De Gennaro V, Frank R. Axisymmetric finite element analysis of pile loading tests. Comput Geotech 2009;36(1-2):6–19. https://doi.org/10.1016/j.compgeo.2008.02.011.

[20] Zabatta R, Govoni L, Foglia A, Mentani A. A simple continuum approach to predict the drained pull-out response of piles for offshore wind turbines. Soils Found 2023;63:101376. https://doi.org/10.1016/j.sandf.2023.101376.

[21] Zhang Y, Ji H, Zhang L, El Naggar MH, Wu W. Identification of bored pile defects utilizing torsional low strain integrity test: Theoretical basis and numerical analysis. J Rock Mech Geotech Eng 2025;17:3035–53. https://doi.org/10.1016/j.jrmge.2024.08.021.

[22] La H, Nguyen T, Pham TA. A novel hybrid metaheuristic-Bayesian machine learning model for accurate load-displacement prediction of pile foundations. Eng Struct 2025;343:121131. https://doi.org/10.1016/j.engstruct.2025.121131.

[23] Mentani A, Govoni L, Bourrier F, Zabatta R. Metamodelling of the load-displacement response of offshore piles in sand. Comput Geotech 2023;159:105490. https://doi.org/10.1016/j.compgeo.2023.105490.

[24] Burd HJ, Taborda DMG, Zdravković L, Abadie CN, Byrne BW, Houlsby GT, Gavin KG, Igoe DJP, Jardine RJ, Martin CM, McAdam RA, Pedro AMG, Potts DM. PISA design model for monopiles for offshore wind turbines: application to a marine sand. Géotechnique 2020;70:1048–66. https://doi.org/10.1680/jgeot.18.P.277.

[25] Byrne BW. Editorial: Geotechnical design for offshore wind turbine monopiles. Géotechnique 2020;70:943–4. https://doi.org/10.1680/jgeot.2020.70.11.943.

[26] Dafalias YF, Manzari MT. Simple plasticity sand model accounting for fabric change effects. J Eng Mech 2004;30(6):622–34. https://doi.org/10.1061/(ASCE)0733-9399(2004)130:6(622).

[27] Schmoor KA, Achmus M, Foglia A, Wefer M. Reliability of design approaches for axially loaded offshore piles and its consequences with respect to the North Sea. Journal of Rock Mechanics and Geotechnical Engineering 2018;10(6):1112–21. https://doi.org/10.1016/j.jrmge.2018.06.004.

[28] Senders, M., 2010. Cone resistance profiles for laboratory tests in sand, in: Proceedings of the 2nd International Symposium on Cone Penetration Testing, Huntington Beach, California, 2-08.

[29] Duncan JM, Seed RB. Compaction-induced earth pressures under K_0 conditions. J Geotech Eng 1986;112:1–22. https://doi.org/10.1061/(ASCE)0733-9410(1986)112:1(1).

[30] Govoni L, Foglia A, Wisotzki E, Quiroz T, Orlando G, Mentani A. Load-displacement response of open-ended piles driven in dense sand under axial compression. Acta Geotech (Rev) 2024.

[31] Lunne T, Robertson PK, Powell JJM. Cone-penetration testing in geotechnical practice. Soil Mech Found Eng 1997;46:237. –237.

[32] Puech A, Foray P. Refined model for interpreting shallow penetration CPTs in sands. Proceeding of Offshore Technology Conference. Huston Texas: OTC; 2002. p. 14257.

[33] Dasseult Systèmes, 2020. Abaqus Analysis User's Manual SIMULIA. Providence, RI, USA.

[34] Randolph MF, Wroth CP. Analysis of Deformation of Vertically Loaded Piles. J Geotech Eng Div 1978;104:1465–88. https://doi.org/10.1061/AJGEB6.0000729.

[35] Han F, Salgado R, Prezzi, M. Lim J. Shaft and base resistance of non-displacement piles in sand. Comput Geotech 2017;83(2017):184–97. https://doi.org/10.1016/j.compgeo.2016.11.006.

[36] Orlando G, Govoni L, Zabatta R, Foglia A. A load-transfer curve formulation to predict the drained response of offshore piles to pull-out, Proceedings of the 9th International Conference of Offshore Site Investigation Geotechnics. London, UK: OSIG; 2023. p. 970–7. https://doi.org/10.3723/WCYG1090.

[37] Hebeler GL, Martinez A, Frost JD. Shear zone evolution of granular soils in contact with conventional and textured CPT friction sleeves. KSCE J Civ Eng 2016;20:1267–82. https://doi.org/10.1007/s12205-015-0767-6.

[38] De Gennaro V, Frank R, Said I. Finite element analysis of model piles axially loaded in sand. Riv Ital di Geotec 2008:45–61.

[39] Tovar-Valencia RD, Galvis-Castro A, Salgado R, Prezzi M. Effect of Surface Roughness on the Shaft Resistance of Displacement Model Piles in Sand. J Geotech Geoenviron Eng 2018;144:04017120. https://doi.org/10.1061/(ASCE)GT.1943-5606.0001828.

[40] Ramadan MI, Butt SD, Popescu R. Offshore anchor piles under mooring forces: numerical modeling. Can Geotech J 2013;50:189–99. https://doi.org/10.1139/cgj-2012-0251.

[41] Lehane BM. Relationships between axial capacity and CPT qc for bored piles in sand. Proceedings of the 5th International Symposium on Deep Foundations on Bored and Auger Piles, 5; 2009. p. 61–74.

[42] White DJ, Bolton MD. Displacement and strain paths during plane-strain model pile installation in sand. Géotechnique 2004;54:375–97. https://doi.org/10.1680/geot.2004.54.6.375.

[43] Li XS, Dafalias YF. Dilatancy for cohesionless soils. Géotechnique 2000;50:449–60. https://doi.org/10.1680/geot.2000.50.4.449.

[44] Richart FE, Hall JR, Woods RD. Vibrations of soils and foundations. International series in theoretical and applied mechanics. Englewood Cliffs, NJ: Prentice-Hall; 1970.

[45] Staubach P, Machaček J, Wichtmann T. Novel approach to apply existing constitutive soil models to the modelling of interfaces. Int J Numer Anal Methods Geomech 2022;46:1241–71. https://doi.org/10.1002/nag.3344.

[46] Chow FC. Investigations into the behaviour of foundation piles for offshore foundations. University of London (Imperial College); 1997.

[47] Jardine RJ, Standing JR, Chow FC. Some observations of the effects of time on the capacity of piles driven in sand. Géotechnique 2006;56(4):227–44.